Millimeter Wave Microstrip Leaky-Wave Antenna Based on SIW and CSRR for Vehicle Application

Feng Gao , Feng-Xiang Li , Bing Wu , Yu-Ying Jin , Guo-Qiang HE *

Posted Date: 14 November 2023

doi: 10.20944/preprints202311.0876.v1

Keywords: Leaky-wave antenna; complementary split resonant ring; low cross-polarization level

Article

Millimeter Wave Microstrip Leaky-Wave Antenna Based on SIW and CSRR for Vehicle Application

Feng Gao [1], Feng-Xiang Li [2], Bing Wu [2], Yu-Ying Jin [2] and Guo-Qiang HE [3,*]

[1] Beijing Zongheng Electromechanical Technology Corporation Limited
[2] School of Communication and Information Engineering, Shanghai University
[3] Key Laboratory of Specialty Fiber Optics and Optical Access Networks and the Joint International Research Laboratory of Specialty Fiber Optics and Advanced Communication, Shanghai University
* Correspondence: ghe@shu.edu.cn

***Abstract*:** A millimeter-wave microstrip leaky-wave antenna array based on the substrate-integrated waveguide (SIW) and the complementary split-ring resonator (CSRR) is proposed in this paper. The slow wave characteristics of the SIW are enhanced by etching two rows of symmetrical CSRR-type slots on the surface of the SIW layer. The magnetic coupling between the CSRR-SIW layer and equally spaced circular patches array on the upper layer realizes the radiation of electromagnetic energy. In the 23~30 GHz (relative bandwidth 26.4%) operating frequency band, the horizontal polarization radiation beam scanning from -62° to -2° is realized, with a peak gain of 9.6~11.7 dBi, and the cross-polarization ratio is more than 43.8 dB.

Keywords: Leaky-wave antenna; complementary split resonant ring; low cross-polarization levels

1. Introduction

WITH the rapid development of radio frequency and wireless communication technologies, there is a growing demand for enhanced antenna design and performance [1]. Among the various types of antennas, leaky-wave antennas stand out as they utilize waveguides or transmission lines as the carrier, control the outward radiation of leaked electromagnetic energy by strategically arranging radiating elements in a periodic manner, and exhibit high integration, compact and stable in structure [2].

Waveguide slotted array antennas were among the earliest forms of leaky-wave antennas. They achieve leakage by cutting slots in the waveguide walls, offering advantages such as simplicity, compactness, high mechanical strength, easy installation and so on. However, they also suffer from drawbacks like high processing difficulty and bulky size, which limit their application in miniaturized and integrated communication systems. Thanks to the emergence of new transmission waveguide structures, leaky-wave antenna design has encountered new opportunities. For example, leaky-wave antennas designed based on the Composite Right/Left-Handed Transmission Line (CRLH) structure have achieved a larger scanning range [3-6]. By employing Substrate Integrated Waveguide (SIW) as opposed to conventional metal waveguide structures, antenna processing costs and weight have been effectively reduced, leading to enhanced performance. SIW, a microwave planar transmission line configuration, comprises periodic arrays of metal-filled vias on a dielectric substrate's both sides. Notably, this innovative structure achieves comparable functionality to that of traditional rectangular waveguides [7]. SIW structures are particularly suited for high-frequency operations, boasting exceptional beam scanning characteristics and directionality. Moreover, they provide the benefits of low loss and seamless integration with circuits, making them highly versatile in antenna [8, 9] and microwave circuit [10] designs. Additionally, leaky-wave antennas operating at millimeter-wave frequencies exhibit remarkable attributes like high resolution, wide bandwidth, and compact size, rendering them extensively employed in various applications, especially in wideband communications.

In 2009, Chiu et al. introduced a slotted array antenna utilizing serpent SIW, which successfully achieved ±30° scanning capabilities across the 23-25 GHz frequency range. This design exhibited

 doi:10.20944/preprints202311.0876.v1

significant advantages over traditional waveguide slotted array antennas, primarily in terms of its low profile and lightweight characteristics. However, it's worth noting that the serpent SIW-based antenna provided a gain range of 8.5-10.5 dBi and relatively higher sidelobe levels [11]. In 2016, Javanbakht et al. introduced a slot leaky-wave antenna utilizing SIW technology, which demonstrated impressive scanning capabilities from 131° to 99° across the 16-19 GHz frequency range [12]. In 2017, Yang et al. presented a wideband continuous transverse stub (CTS) frequency-scanning array antenna, also based on SIW. This particular antenna structure was fed by coaxial probes, while the SIW parabolic reflector facilitated the formation of planar waves. The design incorporated 16 CTS arrays for external radiation, enabling scanning angles from -15.6° to +52.2° within the 8.5-14.1 GHz frequency range [13]. In 2021, Agarwal et al. designed a multi-layer circularly polarized leaky-wave antenna, which incorporated an H-shaped cross slot and a backside circular slot as the radiating elements. This innovative design utilized bevel metal patches, H-shaped cross slots, and SIW to offer Composite Right/Left-Handed (CRLH) characteristics and demonstrated linear polarization beam scanning from -38° to 0° across the 7.6-8.3 GHz frequency range, and circular polarization beam scanning from 0° to +71° within the 8.3-10.6 GHz frequency range with a 3 dB axial ratio bandwidth of 1.8 GHz (8.3-10.1 GHz) and a maximum antenna gain of 9.8 dBi [14].

Leaky-wave antennas have gained significant popularity in communication and radar systems due to their outstanding characteristics. As systems evolve and radio technology moves towards higher frequency bands, this study concentrates on millimeter-wave leaky-wave antennas utilizing SIW technology to meet the escalating demands. The primary objective is to achieve broadband matching and wide-angle scanning. To achieve this, the paper proposes a millimeter-wave microstrip leaky-wave antenna array based on SIW and CSRR (Complementary Split Ring Resonator). The structure is designed with two layers: the bottom layer comprises a slow-wave CSRR-SIW layer featuring etched CSRR-type unit slots, while the top layer contains a circular patch array. Electromagnetic wave radiation is accomplished through magnetic coupling generated within the structure. This innovative design seeks to address the challenges of higher frequency bands and expand the applications of leaky-wave antennas in modern communication and radar systems.

2. Leaky-wave and Antenna Design

A. Analysis and Design of CSRR-SIW Layer Structure

The Substrate Integrated Waveguide (SIW) is chosen as the feeding transmission line structure, and its cut-off frequency is set as 23 GHz. The SIW is designed using a Rogers RO4003 dielectric substrate with properties of $\varepsilon_r = 3.55$, and loss tangent $\tan\delta = 0.0027$, and a thickness of $h_1 = 0.305$ mm. According to the reference [15], the calculated equivalent width w_{eff} of the SIW is 3.5 mm, leading to the fundamental dimensions of $v_d = 0.4$ mm, $v_p = 0.7$ mm, and $d_w = 4.5$ mm for the SIW components.

The proposed antenna configuration is depicted in Figure 1(a) and comprises two distinct layers. The lower layer, referred to as “Sub1”, constitutes the CSRR-SIW layer featuring an open periodic CSRR-type unit slot. For this layer, a Rogers RO4003 dielectric substrate with a thickness of $h_1 = 0.305$ mm is employed. The Feeding line is structured as a 50 Ω microstrip line, and a specially designed trapezoidal taper structure ensures effective impedance matching between the SIW and the 50 Ω excitation port. On the other hand, the upper layer, labeled “Sub2”", employs circular patches arranged at even intervals to serve as the radiating layer. This layer utilizes an F4B dielectric substrate with properties of $\varepsilon_r = 2.65$ and $\tan\delta = 0.001$, and it has a thickness of $h_2 = 0.5$ mm. The two layers of dielectric substrates are directly connected without any air layer in between, facilitating a tightly integrated antenna structure.

Preprints (www.preprints.org) | NOT PEER-REVIEWED | Posted: 14 November 2023 doi:10.20944/preprints202311.0876.v1

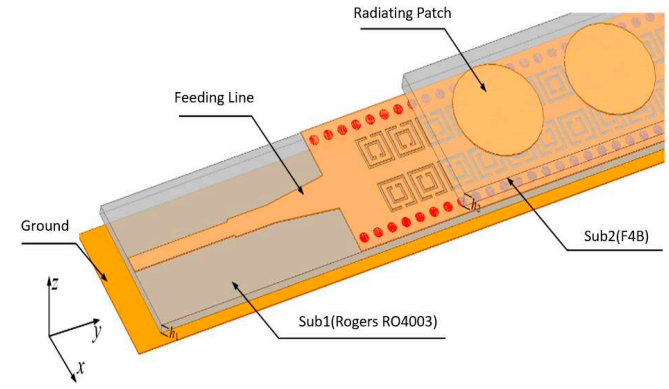

（a）3D structure diagram

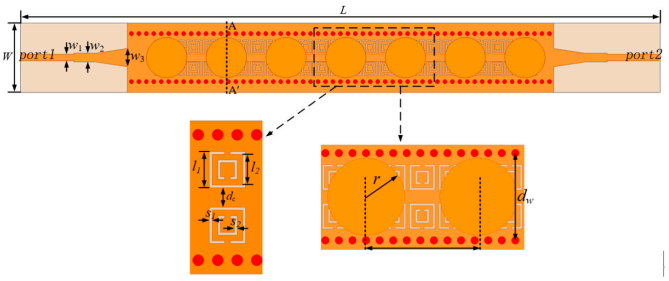

（b）top view

Figure 1. Schematic diagram of the microstrip leaky-wave antenna structure based on SIW and CSRR.

Figure 1(b) illustrates the top view of the designed antenna structure, featuring a CSRR-SIW layer with two CSRR-type radiating slots symmetrically etched above the SIW structure. The effects of parameters such as l_1, d_c, s_1, and s_2 on the transmission characteristics of the CSRR-SIW layer were analyzed using the HFSS simulation software.

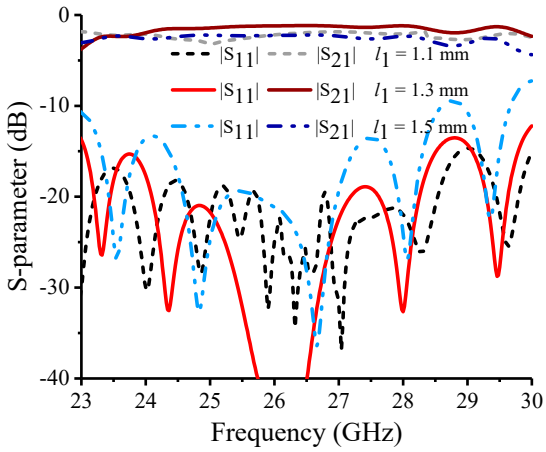

Figure 2. Relationship between the S-parameters of the CSRR-SIW layer and the length (l_1) of the outer metal strip of the CSRR.

Figure 2 presents the simulated reflection coefficient |S11| and transmission coefficient |S21| of the CSRR-SIW layer, showcasing the relationship with the outer ring metal strip length, l_1. When the

Preprints (www.preprints.org) | NOT PEER-REVIEWED | Posted: 14 November 2023 doi:10.20944/preprints202311.0876.v1

other structure parameters remain constant, an increase in the length l_1 of the outer ring metal strip results in a gradual broadening of the matching bandwidth for the CSRR-SIW layer.

The spacing (d_c) between the symmetrically placed CSRR units also plays a significant role in influencing the transmission characteristics of the CSRR-SIW layer. Figure 3 illustrates the impact of the spacing (d_c) on the S-parameters of the CSRR-SIW layer. While keeping the other parameters constant, it is observed that given d_c as 0.5 mm enables the CSRR-SIW layer having a frequency band with |S11| > -10 dB at both low and high frequencies.

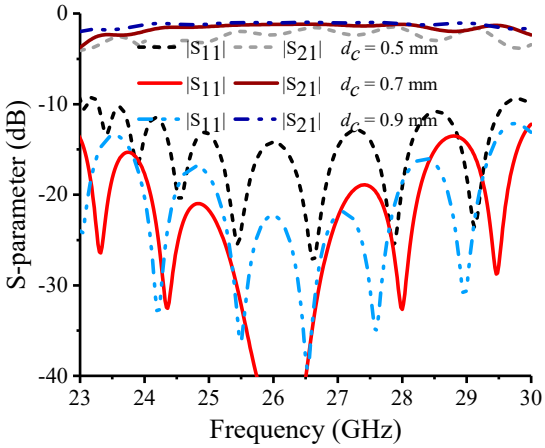

Figure 3. Variation curve of the S-parameters of the CSRR-SIW layer with changes in the spacing (d_c) between the CSRR units that are symmetrically placed.

As the value of d_c is increased from 0.5 mm to 0.9 mm, the reflection coefficient |S11| gradually decreases, leading to a broader matching bandwidth. When d_c is chosen as 0.7 mm, |S11| drops below -12.5 dB within the frequency range of 23~30 GHz. This indicates that the CSRR-SIW layer exhibits favorable transmission characteristics at this specific spacing value.

Figure 4 demonstrates the influence of the CSRR inner slot width (s_1 and s_2) on the S-parameters of the CSRR-SIW layer. While maintaining the other parameters constant, it can be observed that as the values of s_1 and s_2 increase from 0.06 mm to 0.12 mm, the curves of |S11| and |S21| exhibit only minor fluctuations. This suggests that s_1 and s_2 have minimal effects on the transmission characteristics of the CSRR-SIW layer.

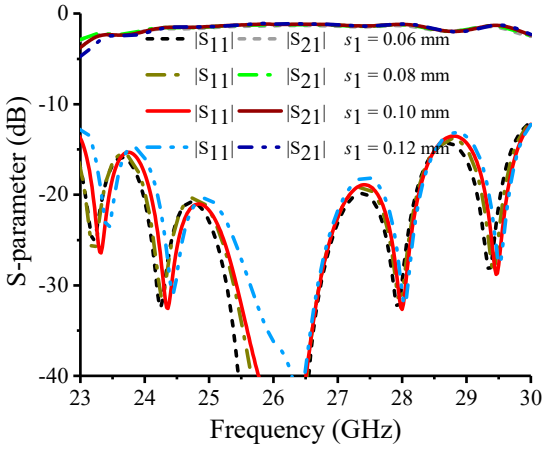

（a）The S parameters under different values of s1

Preprints (www.preprints.org) | NOT PEER-REVIEWED | Posted: 14 November 2023 doi:10.20944/preprints202311.0876.v1

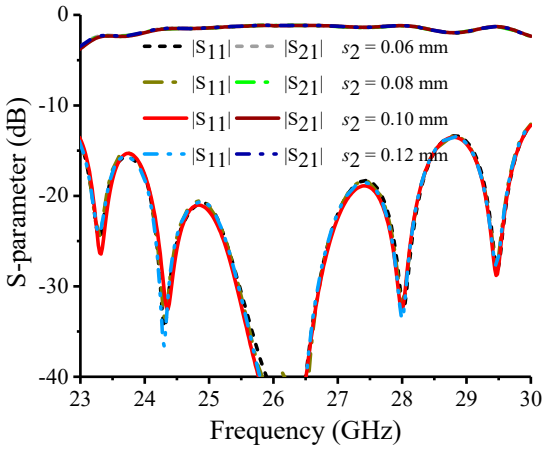

（b）The S parameters under different values of s2

Figure 4. Relationship between the S-parameters of the CSRR-SIW layer and the CSRR inner slot widths (s_1 and s_2).

Therefore, when the waveguide width (d_w) of SIW remains unchanged, the primary factors affecting the transmission characteristics of the CSRR-SIW layer are the length l_1 of the CSRR unit edge and the spacing d_c between the symmetrically placed CSRR units. Other parameters, such as s_1 and s_2, have a relatively limited impact on the overall performance of the CSRR-SIW layer in terms of S-parameters.

In Figure 5, the electric field distribution of two structures, namely an SIW and a CSRR-SIW layer with etched CSRR-type slots of the same size, is presented at the central frequency of 26.5 GHz. It is evident that the SIW structure operates in the TE_{10} mode, displaying eight electric field periods inside the waveguide.

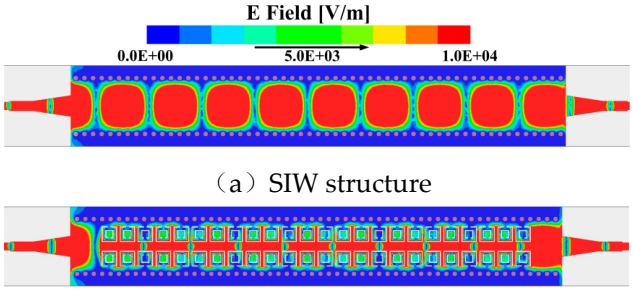

（a）SIW structure

（b）CSRR-SIW layer

Figure 5. Electric field distribution of the SIW structure and the CSRR-SIW layer at 26.5 GHz.

On the other hand, the CSRR-SIW layer exhibits nine electric field periods, indicating that its waveguide wavelength is shorter, leading to a larger phase constant. This observation confirms that the slow-wave characteristics of the SIW structure are enhanced by etching CSRR-type slots on the surface of the SIW. The presence of the CSRR-type slots introduces additional periodicity, resulting in a shorter wavelength and larger phase constant, thus validating the improved slow-wave behavior in the CSRR-SIW layer compared to the standard SIW structure.

In Figure 6, the radiation pattern of the CSRR-SIW layer is depicted. The polarization pattern shown in Figure 6(a) indicates that the CSRR-SIW layer does not possess frequency scanning functionality within the frequency range of 23~30 GHz. Furthermore, the maximum gain in the main polarization direction is merely -2.5 dBi, and the cross-polarization level is below -35.4 dBi.

Preprints (www.preprints.org) | NOT PEER-REVIEWED | Posted: 14 November 2023 doi:10.20944/preprints202311.0876.v1

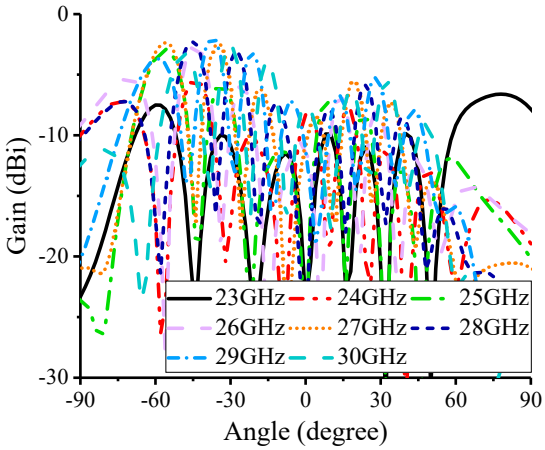

（a）main polarization

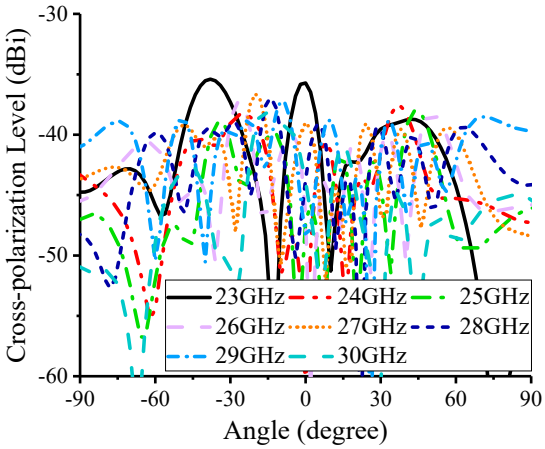

（b）cross-polarization

Figure 6. Simulated radiation pattern of the CSRR-SIW layer.

Based on the analysis of the structural parameters of the CSRR-SIW layer and the observation of the electric field distribution, it can be inferred that the CSRR-SIW layer primarily functions in transmission and feeding roles. To achieve electromagnetic energy radiation effectively, additional radiation elements need to be integrated into the structure. The current CSRR-SIW layer acts as a transmission medium rather than an active radiating element, contributing to the overall functionality of the antenna structure.

B. Antenna Performance Analysis

Circular patches are widely used as radiating elements in antenna design due to their straightforward structure, and they are particularly common in microstrip patch antennas. The fundamental mode of circular patches is the TM_{11} mode. The radius (r) of the circular radiating patch can be approximately calculated using the following formula [16]:

$$r = \frac{1.841184c}{2\pi f_0 \sqrt{\varepsilon_r}} \tag{1}$$

In this paper, the circular patches are arranged in the upper layer to form an equidistant linear array, with a total of 7 circular patches. The spacing between adjacent patches is set to $d_r = \lambda_g/2 = 5.6$ mm, where λ_g represents the waveguide wavelength calculated using formula (6).

Preprints (www.preprints.org) | NOT PEER-REVIEWED | Posted: 14 November 2023 doi:10.20944/preprints202311.0876.v1

In Figure 7(a) and (b), the magnetic field distribution on the AA' plane of the CSRR-SIW layer is illustrated before and after loading the radiating patches, respectively. At the frequency of 26.5 GHz, in the absence of the radiating patches, the magnetic field is tightly confined to the SIW layer, and magnetic coupling occurs between the symmetrically placed CSRR units. Consequently, the magnetic field distribution above the SIW layer gradually weakens.

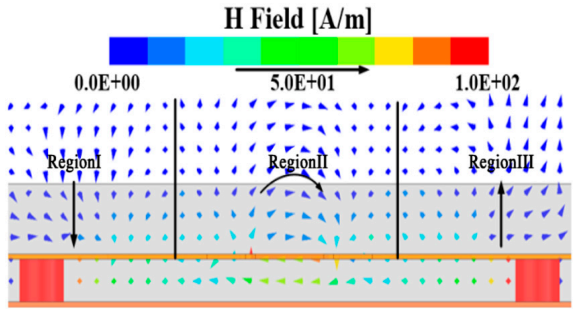

（a）before loading

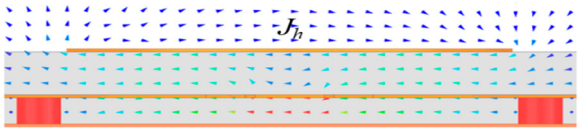

（b）after loading

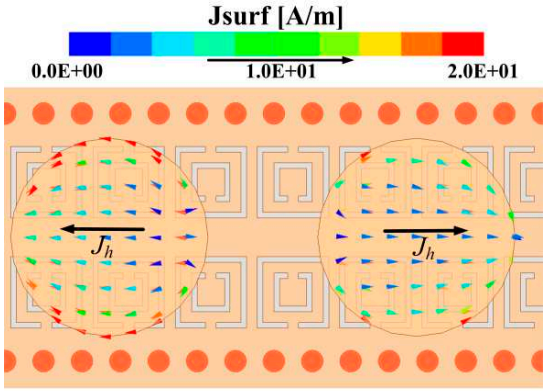

（c）the surface current distribution

Figure 7. Simulated the magnetic field distribution on the AA′ plane and the surface current distribution on the circular radiating patches before and after loading at 26.5 GHz.

Via loading the radiating patches, a notable interaction arises between the out-of-phase magnetic field components in regions I and III and the radiating patches. This interaction induces a horizontal induced current (J_h) on the surface of the radiating patches.

The introduction of the radiating patches alters the magnetic field distribution, leading to the creation of induced currents on the patches' surfaces. These induced currents contribute to the radiation of electromagnetic energy, enhancing the overall performance of the antenna by providing radiation capabilities that were absent in the initial CSRR-SIW layer configuration. The induced horizontal current (J_h) flows along the surface of the metal patches, resulting from the interaction between the out-of-phase magnetic field components in regions I and III and the radiating patches. This current significantly enhances the magnetic field in regions I and III compared to the situation without the patches. This enhancement indicates a strong coupling between the radiating patches and the energy radiated by the SIW in the lower layer. The current distribution as shown in Figure 7(c) is horizontal along the surface, indicating that the antenna radiates horizontally polarized waves. The induced current on the circular radiating patches facilitates the emission of electromagnetic

Preprints (www.preprints.org) | NOT PEER-REVIEWED | Posted: 14 November 2023 doi:10.20944/preprints202311.0876.v1

energy in a horizontal polarization, making the antenna suitable for radiating horizontally polarized signals. This is a desirable characteristic for many communication applications.

Based on the analysis discussed earlier, the magnetic field coupling within the structure leads to the radiation of horizontally polarized waves. However, to achieve high purity of horizontally polarized waves, it is necessary to suppress electric field coupling. Figure 9 illustrates the electric field distribution on the AA' plane before and after loading the circular radiating patches at the frequency of 26.5 GHz. It's shown that there is no significant change in the electric field distribution on the AA' plane before and after loading the patches. This lack of change indicates that the electric field coupling has been effectively suppressed. By mitigating electric field coupling, the antenna can achieve a high level of purity in the horizontally polarized waves, ensuring improved performance for specific applications that require high cross polarization ratio.

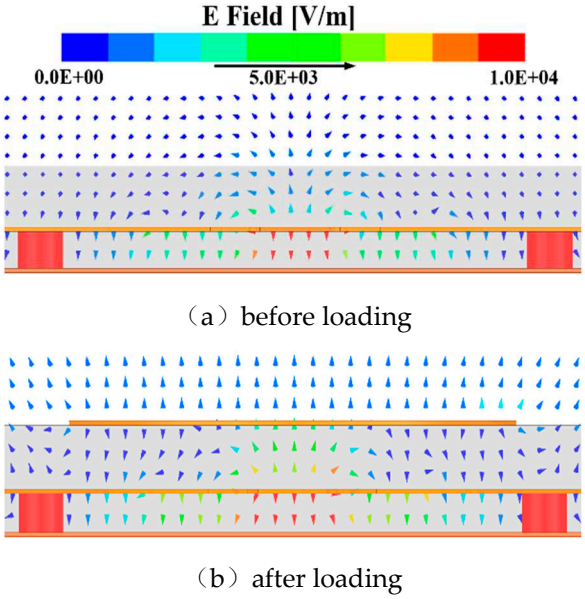

Figure 9. Displays the electric field distribution on the AA' plane before and after loading the radiating patches at 26.5 GHz.

The impact of different upper-layer substrate materials with varying relative permittivity (ε_r) on the overall antenna structure's S-parameters and peak gain was analyzed. Figure 10 and Figure 11 display the simulated S-parameters and peak gains of the various antenna structures using different upper-layer substrate materials: Rogers RT5880 with ε_r = 2.2, F4B with ε_r = 2.65, and Rogers RO4003 with ε_r = 3.55 (the same material as the CSRR-SIW layer). From the analysis of Figure 10, it becomes evident that as the relative permittivity of the upper-layer substrate decreases, the matching bandwidth with |S11| < -10 dB gradually widens, particularly at lower frequencies. Additionally, the minimum position of the |S21| curve shifts towards higher frequencies as ε_r decreases.

Turning to Figure 11, it demonstrates that when using a substrate material with ε_r = 2.2, the peak gain exhibits more significant fluctuations, while using a substrate material with ε_r = 3.55 leads to a lower gain. The reduced gain in the latter case can be attributed to increased losses at higher frequencies due to the higher permittivity of the substrate.

Based on these observations, the upper-layer substrate material with ε_r = 2.65 (F4B) is chosen for the radiating layer. This selection is made to achieve a balance between wider bandwidth with good matching and a stable peak gain performance. The chosen substrate material ensures efficient radiation with reduced losses at higher frequencies, making it the optimal choice for the specific application of the antenna.

Preprints (www.preprints.org) | NOT PEER-REVIEWED | Posted: 14 November 2023 doi:10.20944/preprints202311.0876.v1

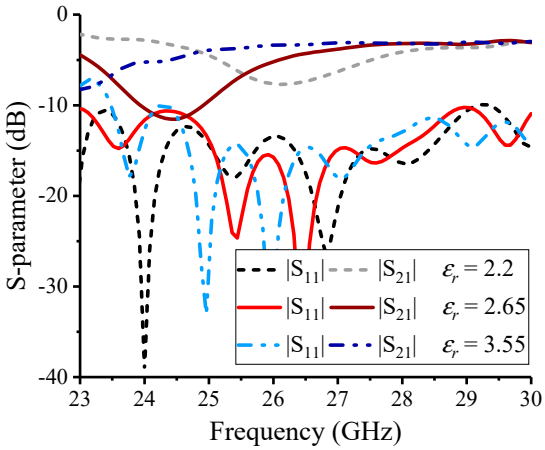

Figure 10. Impact of using upper-layer substrates with different relative permittivity (εr) on the antenna S-parameters

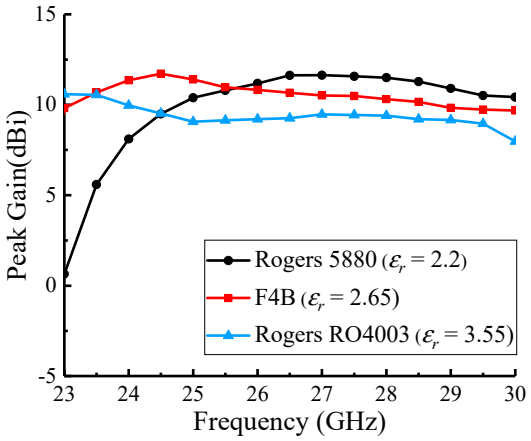

Figure 11. Comparison of simulated antenna peak gain for different upper-layer substrates with varying relative permittivity (εr).

3. Antenna Simulation Results and Analysis

After optimizing and analyzing various parameters of the antenna structure as described above, Table 1 provides the optimal values of the structural parameters for the millimeter-wave microstrip leaky-wave antenna based on SIW and CSRR. The overall dimensions of the antenna are $L \times W \times H$ = 60 mm × 6.5 mm × 0.805 mm = $5.3\lambda_0 \times 0.57\lambda_0 \times 0.07\lambda_0$ (where H is the total thickness of the antenna structure).

Table 1. The key geometric parameters of a leaky-wave antenna (units ： mm).

Parameters	*h1*	*h2*	*w1*	*w2*	*w3*	*l1*	*l2*
Values	0.305	0.50	0.62	0.80	1.70	1.30	1.10
Parameters	*s1*	*s2*	*dc*	*r*	*dr*	*dw*	
Values	0.10	0.10	0.70	1.90	5.60	4.50	

When port 1 of the structure shown in Figure 1 is excited with a feeding signal and port 2 is connected to a matching load, the simulated reflection coefficient in dB of the millimeter-wave microstrip leaky-wave antenna based on SIW and CSRR are shown in Figure 12. The results indicate

Preprints (www.preprints.org) | NOT PEER-REVIEWED | Posted: 14 November 2023 doi:10.20944/preprints202311.0876.v1

that within the frequency range of 23 GHz to 30 GHz, $|S_{11}| < -10$ dB,, which demonstrates that the designed antenna achieves good matching over a wide bandwidth of 7 GHz (relative bandwidth of 26.4%).

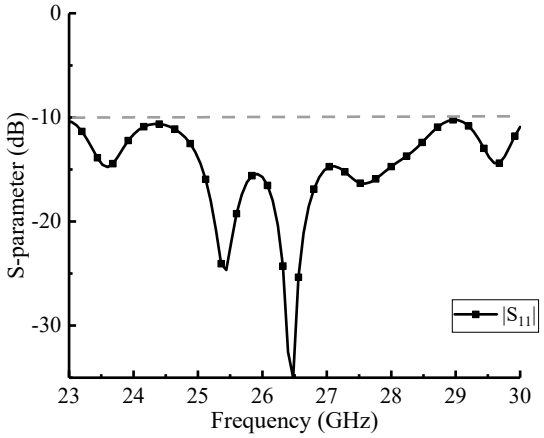

Figure 12. Simulated S-parameters of the millimeter-wave microstrip leaky-wave antenna based on SIW and CSRR.

Based on the analysis from Figure 7, it has been established that the designed microstrip leaky-wave antenna based on SIW and CSRR effectively radiates horizontally polarized waves. Figure 14(a) and (b) present the simulated radiation patterns for the main polarization and cross-polarization, respectively.

Within the operating frequency range of 23 GHz to 30 GHz, the antenna exhibits a scanning range from -62° to -2°, demonstrating the capability to cover a wide angular range. Furthermore, the antenna achieves a gain greater than 9.6 dBi, which ensures strong signal reception and transmission. Additionally, the cross-polarization level is lower than -33.4 dBi, indicating a high level of purity in the horizontally polarized waves and efficient suppression of cross-polarized radiation.

The combined performance of wide scanning range, high gain, and low cross-polarization makes this microstrip leaky-wave antenna a promising candidate for various millimeter-wave communication and radar applications, where precise beam scanning and high-quality radiation characteristics are essential.

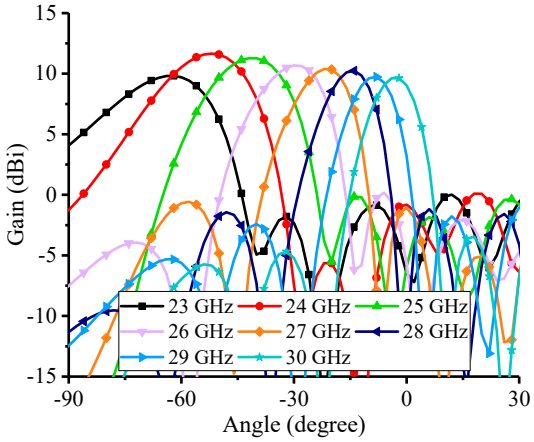

(a) main polarization

Preprints (www.preprints.org) | NOT PEER-REVIEWED | Posted: 14 November 2023 doi:10.20944/preprints202311.0876.v1

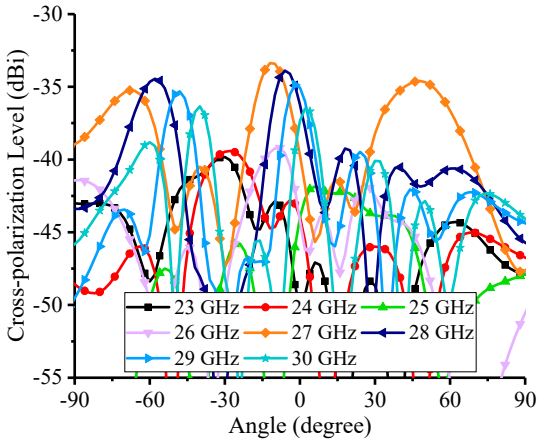

(b) cross-polarization

Figure 13. Simulated radiation patterns of the millimeter-wave microstrip leaky-wave antenna based on SIW and CSRR for both main polarization and cross-polarization.

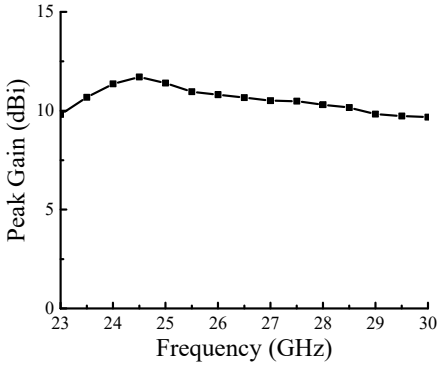

Figure 14. Peak gain and radiation efficiency of the millimeter-wave microstrip leaky-wave antenna based on SIW and CSRR.

Figure 14 shows the peak gain and radiation efficiency of the designed leaky-wave antenna. Within the frequency range of 23 GHz to 30 GHz, the peak gain varies from 9.6 dBi to 11.7 dBi. The minimum gain of 9.6 dBi is obtained at 30 GHz, while the maximum gain of 11.7 dBi is achieved at 24.5 GHz. The antenna exhibits a minimum and maximum radiation efficiency of 43% and 81%, respectively, corresponding to the frequencies of 30 GHz and 24.5 GHz.

4. Conclusion

This paper presents a novel millimeter-wave microstrip leaky-wave antenna based on SIW and CSRR. The antenna design utilizes a planar SIW transmission structure, which offers advantages such as light weight, low profile, and ease of integration with other components. The antenna achieves good impedance matching with $|S11| < -10$ dB within the frequency range of 23 GHz to 30 GHz, corresponding to a relative bandwidth of 26.4%. Moreover, the antenna accomplishes a wide scanning angle of 60°. The performance of the designed antenna is remarkable, with peak gain varying from 9.6 dBi to 11.7 dBi, and a high cross-polarization ratio greater than 43.8 dB. These characteristics highlight the antenna's excellent beam scanning capabilities and high polarization purity, making it well-suited for applications in the high-frequency communication, especially for vehicle platform.

Acknowledgments: This work is supported by research on wireless communication technology of train network control system, Science and Technology Research and Development Plan of China Academy of Railway Sciences Corporation Limited, Contract No. L2021J002. National Natural Science Foundation of China (NSFC) under Grant No. 62001280, 111 Project (D20031), Guangxi Key Laboratory of Wireless Wideband Communication and Signal Processing (GXKL06200213).

References

1. KARIMIPOUR M, KOMJANI N. Realization of multiple concurrent beams with independent circular polarizations by holographic reflectarray[J]. IEEE Transactions on Antennas and Propagation, 2018, 66(9): 4627-4640.
2. GRBIC A, ELEFFHERIADES G V. Leaky CPW-based slot antenna arrays for millimeter-wave applications[J]. IEEE Transactions on Antennas and Propagation, 2002, 50(11): 1494-1504.
3. LAI A, ITOH T, CALOZ C. Composite right/left-handed transmission line metamaterials [J]. IEEE Microwave Magazine, 2004, 5(3): 34-50.
4. LIM S, CALOZ C, ITOH T. Metamaterial-based electronically controlled transmission-line structure as a novel leaky-wave antenna with tunable radiation angle and beamwidth[J]. IEEE Transactions on Microwave Theory and Techniques, 2004, 52(12): 2678-2690.
5. SAGHATI A P, MIRSALEHI M M, NESHATI M H. A HMSIW circularly polarized leaky-wave antenna with backward, broadside, and forward radiation[J]. IEEE Antennas and Wireless Propagation Letters, 2014, 13: 451-454.
6. HAGHIGHI S S, HEIDARI A, MOVAHHEDI M. A three-band substrate integrated waveguide leaky-wave antenna based on composite right/left-handed structure[J]. IEEE Transactions on Antennas and Propagation, 2015, 63(10): 4578-4582.
7. DESLANDE D, WU K. Integrated microstrip and rectangular waveguide in planar form[J]. IEEE Microwave and Wireless Components Letters, 2002, 11(2): 68-70.
8. LUO G Q, HU Z F, DONG L X, et al. Planar slot antenna backed by substrate integrated waveguide cavity[J]. IEEE Antennas and Wireless Propagation Letters, 2008, 7: 236–239.
9. HESARI S S, BORNEMANN J. Wideband circularly polarized substrate integrated waveguide endfire antenna system with high gain[J]. IEEE Antennas and Wireless Propagation Letters, 2017, 16: 2262-2265.
10. MARTINEZ J A, DE DIOS J J, BLENGUER A, et al. Integration of a very high quality factor filter in empty substrate-integrated waveguide at Q-band[J]. IEEE Microwave and Wireless Components Letters, 2018, 28(6): 503–505.
11. CHIU L, HONG W, KUAI Z. Substrate integrated waveguide slot array antenna with enhanced scanning range for automotive application[C]. 2009 Asia Pacific Microwave Conference, 2009: 1-4.
12. JAVANBAKHT N, MAJEDI M S, ATTARI A R. Periodic leaky-wave antenna with transverse slots based on substrate integrated waveguide[C]. 2016 24th Iranian Conference on Electrical Engineering (ICEE), Shiraz, Iran, 2016, pp. 608-612,.
13. YANG X X, DI L Q, YU Y J, GAO S. Low-profile frequency-scanned antenna based on substrate integrated waveguide[J]. IEEE Transactions on Antennas and Propagation, 2017, 65(4): 2051-2056.
14. AGARWAL R, YADAVA R L, DAS S. A multilayered SIW-based circularly polarized CRLH leaky wave antenna[J]. IEEE Transactions on Antennas and Propagation, 2021, 69(10): 6312-6321.
15. NIEMBRO M A, NASSERDDINE V, PISTONO E, et al. Slow-wave substrate integrated waveguide[J]. IEEE Transactions on Microwave Theory and Techniques, 2014, 62(8): 1625–1633.
16. BALANIS C A. Antenna theory analysis and design[M]. 4rd Ed., New York: John Wiley & Sons, Inc, 2016.